Changes in extreme precipitation over Spain using statistical downscaling of CMIP5 projections

Robert Monjo[1], Emma Gaitán[1], Javier Pórtoles[1], Jaime Ribalaygua[1], Luis Torres[1]

[1]Climate Research Foundation (FIC)
C/ Tremps 11, Madrid 28040, Phone: +34 91 521 01 11
e-mail: rma@ficlima.org

IMPORTANT*: This is the pre-peer reviewed version of the following article:* Monjo R, Gaitán E, Pórtoles J, Ribalaygua J, Torres L. 2015. Changes in extreme precipitation over Spain using statistical downscaling of CMIP5 projections*. Int J Climatol,* doi: 10.1002/joc.4380***, which has been published in final form at http://doi.org/10.1002/joc.4380.***

Abstract The Mediterranean coast of Spain often experiences intense rainfall, sometimes reaching remarkable amounts of more than 400 mm in one day. The aim of this work is to study possible changes of extreme precipitation in Spain for this century, simulated from several CMIP5 climate models. Eighteen climate projections (9 models under RCP4.5 and RCP8.5 scenarios) were downscaled using a two-step analogue/regression statistical method. We have selected 144 rain gauges as the rainiest of a network by using a threshold of 250 mm in one day for a return period of 100 years. Observed time-series have been extended using the ERA40 reanalysis and have subsequently been used to correct the climate projections according to a parametric quantile-quantile method. Five theoretical distributions (Gamma, Weibull, Classical Gumbel, Reversed Gumbel and Log-logistic) have been used to fit the empirical cumulative functions (entire curves, not only the upper tail) and to estimate the expected precipitation according to several return periods: 10, 20, 50 and 100 years. Results in the projected changes for 2051-2100 compared to 1951-2000 are similar (in terms of sign and value) for the four return periods. The analyzed climate projections show that changes in extreme rainfall patterns will be generally less than the natural variability. However, possible changes are detected in some regions: decreases are expected in a few kilometres inland, but with a possible increase in the coastline of southern Valencia and northern Alicante, where the most extreme rainfall was recorded. These results should be interpreted with caution because of the limited number of climate projections; anyway, this work shows that the developed methodology is useful for studying extreme rainfall under several climate scenarios.

Keywords: climatic change, extreme precipitation, rainfall, statistical downscaling, CMIP5, Spain.

1 Introduction

The Mediterranean climate is characterized by a high variability of the rainfall patterns, occasionally including both long periods of drought and extraordinary rainfall events (Pérez-Cueva, 1983, Llasat *et al.*, 1996, Font-Tullot, 2000). The east of the Iberian Peninsula is one of the Mediterranean regions where highest rainfall values have been recorded. In most cases, extreme rain is caused by deep convection of highly organized systems, which are generated in a synoptic environment of forcing for ascent (Lazier *et al.*, 2001). One item that usually appears in that synoptic situations is the *cut-off low* (closed upper-level low), popularly known as *Gota Fría* in Spain (Armengot-Serrano 1994).

Several studies on extreme events in this area have shown that precipitation expected in a day, for a return period of 100 years, exceeds 400 mm in some cases (De Luís, 2000, Egozcue and Ramis, 2001). The highest values include the official record of 817 mm in Oliva (Valencia) on 1987, November 3rd (Armengot-Serrano, 1994, AEMet, 2007, Ramis *et al.*, 2013). The south-eastern coast of the peninsula is one of the areas that have experienced extraordinary rainfall – we highlight the 600 mm in a few hours in Almeria on 1973, October 17th (Gil and Olcina, 1999). But several significant flood episodes have also been recorded in the northern coast of Spain, one of them out of the ordinary, floods in Bilbao in 1983 (Ugarte and Gonzalez, 1984), with 503 mm recorded in one day.

Moreover, local adaptation policies to climate change require the possible evolution of extreme rainfall to minimize flooding risks and its consequences. Nevertheless, there are significant uncertainties in the future evolution of extreme rainfall due to several sources: climate simulations (emission scenarios and climate models), methods of extreme rainfall estimation and large natural variability of precipitation. Theoretically, most of these uncertainties can be partially quantified by using a large number of climate projections. However, deep convection is poorly simulated by global models (Herrmann 2008), and therefore climate models need to be downscaled to better detect deep convection.

In the statistical downscaling approach, high-resolution predictands are obtained by applying to the climate models outputs a set of relationships previously identified in the observed climate between these predictands and large-scale predictors (Imbert and Benestad, 2005).

Thanks to the CMIP5 (Coupled Model Intercomparison Project Phase 5), a set of atmosphere-ocean global climate models have been made available for its use in climatic studies. One of the core simulations within the suite of CMIP5 long-term experiments are the *historical* runs which cover much of the industrial period (1850 - at least 2005) and that can be referred to as "twentieth century" simulations (Taylor *et al.*, 2012). They are forced by observed atmospheric composition changes (reflecting both anthropogenic and natural sources) and, for the first time, including time-evolving land cover. These *historical* runs have a key role for our work: they allow us to evaluate model performance against present climate (Taylor *et al.*, 2009).

Precipitation outputs obtained directly from CMIP5 models show serious problems to reproduce the extreme values, which are mainly due to its insufficient spatial resolution. Precipitation simulated by the ERA40 Re-Analysis presents similar problems. For this reason, a statistical downscaling is required in order to simulate a better probability distribution of precipitation at local scale. One of the methods that have obtained better results in Spain is the two-step analogue/regression technique, developed by Ribalaygua *et al*. (2012) and validated for Europe (Linden and Mitchell 2009, Goodess et al. 2011).

The aim of this work is to study the projected evolution of extreme precipitation in Spain for the next 100 years by using several downscaled CMIP5 climate models. However, extreme values associated with empirical return periods have a large error because they are estimated with very few values of precipitation. For example, the highest value in a time-series has never been surpassed, so its empirical return period is infinity. In addition, most time-series are shorter than ten years. For all these reasons, the use of theoretical functions is required to extrapolate return periods. Some theoretical distributions are able to fit the entire set of empirical values, including zero values (Moncho *et al.*, 2012). Thus, the possible overshooting of the end of the accumulated probability curve is greatly reduced.

2 Study area and data

2.1 Study area

In this study we analyze the most extreme rainfall area of Spain, which is found mainly on the Mediterranean coast (including Balearic Islands) and, with a lesser extent, in some parts of northern and inner Iberian Peninsula. Mediterranean climate prevails in most of the studied area

except on the northern peninsula, which has a strong influence of oceanic climate (Capel-Molina, 2000, Martín-Vide and Olcina, 2001). Extreme monthly precipitation can have values ranging from a total amount of 0 mm (in July in some south-eastern areas) to almost 1000 mm in northern areas. This value is also measured sometimes on the Mediterranean coast, where a high amount of precipitation in only a few days is usually recorded (Martín-Vide, 2004). This area is located in the north of Alicante and in the south of Valencia provinces, and has special interest because it also holds the record for Spain of rainfall in a day (817 mm).

2.2 Observations data

A group of rain gauges belonging to the Spanish Meteorological Agency (AEMet) has been selected by a two stages process. First, a group of 5,217 rain gauges was chosen by limiting its length to at least 3,600 daily records within the used common period with the ERA40 reanalysis (1958-2000). In the second stage, we selected the rain gauges that have recorded the most intense precipitations in Spain. In particular, we chose the threshold of 250 mm in a day for a return period of 100 years (i.e. centile 99.99726), and thus 144 rain gauges were found (Fig. 1). This theoretical return period has been considered in order to compare the extreme probability in the larger time-series (43 years) and the shorter time-series (10 years).

2.3 Climate Models data

We have used data from nine CMIP5 climate models, supplied by the Program for Climate Model Diagnosis and Intercomparison (PCMDI) archives. The climate models (Table 1) were selected according to the time resolution (daily) of available predictor fields, because it is required for the used downscaling method (see section 3.1). In particular, daily averages of the geopotencial height at 1000 and 500 hPa were used to calculate geostrophic winds (predictors) for both the *historical* simulation and for two future climate projections corresponding to the Representative Concentration Pathways RCP4.5 and RCP8.5 (Taylor *et al.*, 2009). The *raw* output has been used, i.e. the data are used as they are provided without any treatment (bias correction or any other processing). Only the *raw* output was chosen because models do not have the same number of runs, and it should not give more weight to a type of simulation than to other. Every model has its own defined grid and a calendar of its choice.

2.4 Reanalysis data

In order to study the behaviour of the CMIP5 models *historical* simulations, we have used the ECMWF (European Centre for Medium-Range Weather Forecasts) ERA40 Re-Analysis (Uppala *et al.*, 2005) for the 1958-2000 period. The same large-scale fields than for CMIP5 were taken from the ERA40 Re-Analysis (geopotencial height at 1000 and 500 hPa). The Re-Analysis has a reduced Gaussian grid with approximately uniform 125 km spacing. In our work, the original ERA40 grid has been interpolated (by using the Bessel interpolation applied to 16 points) to the grids used by each one of the climate models to be downscaled. The limits of the used atmospheric window are 31.500ºN to 55.125ºN latitude and 27ºW to 14.625ºE longitude; this window has been defined trying to cover both the geographic area under study as well as the surrounding areas with meteorological influence on the Iberian Peninsula.

3 Methodology

3.1 Downscaling method

This work uses the two-step analogue/regression statistical downscaling method developed by Ribalaygua et al. (2012). A brief summary of the two-step method is presented in this section.

The first step is an analogue stratification (Zorita and von Storch, 1999): the *n* most similar days to the day to be downscaled are selected. The similarity between two days was measured using a weighted Euclidean distance according to three nested synoptic windows and four large-scale fields used as predictors: (1) speed and (2) direction of the geostrophic wind at 1000 hPa and (3) speed and (4) direction of the geostrophic wind at 500 hPa. For each predictor, the distance was calculated and standardised by substituting it by the closest centile of a reference population of distances for that predictor. The four predictors were finally equally weighted, while the synoptic windows had different weights.

In the second step, we downscale together a group of *m* problem days (we use the whole days of a month). For each problem day we obtain a "preliminary precipitation amount" averaging the rain amount of its *n* most analogous days, so we can sort the *m* problem days from the highest to the lowest "preliminary precipitation amount". And for assigning the final amount of rain, we take each of the amounts of rain of the $m \times n$ analogous days, then we sort those $m \times n$ amounts of rain and then we cluster those amounts in *m* groups; every quantity is then assigned, orderly, to the *m* days previously sorted by the "preliminary precipitation amount". An example of this is shown in Table 2.

The first and second steps of the downscaling method are linked: particularly, the choice of *m* depends on the value of *n*. It is assumed that the climatic characteristics of rainfall vary little within a month. For this reason, the $n \times m$ analogous days of a month can be mixed in order to obtain a better ECDF, i.e. with tails less smoothed. Therefore, the number of problem days is chosen as $m = 30$, and the number of analogous days (*n*) was selected based on this assumption.

Several tests were previously performed to find the best *n* for this work. The analogue stratification obtained similar Ranking Probability Score (RPS about 8%) for values of *n* between 20 and 40 analogous per day. Therefore, the second step was crucial to determine the best *n*: If the population of analogues (*n*) exceeds the number of problem days (*m*), the final precipitation is too smooth (underestimates heavy rain and dry days) due to the average per problem day. The probability distribution of the simulated precipitation is more similar to that observed when *n* is smaller because its average is least smooth. In theory, it is expected that $n = 1$ obtains the highest similarity in the empirical cumulative distribution (ECDF). However, the RPS is better for *n* higher than 20 and therefore we chosen $n = m = 30$. This case is an optimum value even compared with the ECDF simulated with $n = 1$, at least according to the Anderson Darling test (Ribalaygua *et al.*, 2012).

3.2 Cumulative Probability Functions

The cumulative probability distribution (π) is the function that describes the probability of registering a daily precipitation equal or minor than *p*, i.e., the sum of frequency of days with a precipitation equal or minor than *p*. We can distinguish between empirical and theoretical distributions: If the curve is estimated from a time series of precipitation (observed or simulated), we will refer to an *empirical cumulative distribution function* (ECDF). However, if the curve is obtained by a theoretical mathematical function, we refer to it as *theoretical cumulative distribution function* (TCDF). For simplicity, all theoretical functions that we have considered require a standard precipitation, λ, defined as:

$$\lambda(p; P_o, P_1) \equiv \frac{p - P_o}{P_1} \qquad \text{Eq. 1}$$

where *p* is the daily precipitation. The parameter P_o is the most probable value and P_1 is the scale factor. Both parameters depend on the probability distribution used. We have chosen theoretical distributions able to fit the entire set of empirical values, including the zeros. Thus, the possible overfitting of the end of the probability curve is greatly reduced. In particular, we have used several probability distributions, based on four-parametric versions $\pi(p; P_o, P_1, w, h)$ of five

distributions (Eq. 2 to 6): Gamma, Weibull, Classical Gumbel, Reverse Gumbel and Modified Log-logistic (Moncho *et al.*, 2012).

$$\pi_1 = \frac{\gamma\left(h, \lambda^w\right)}{\Gamma\left(h\right)} \quad \text{Eq. 2}$$

$$\pi_2 = 1 - \exp\left(-\lambda^w - h\right) \quad \text{Eq. 3}$$

$$\pi_3 = \exp\left[-\exp\left(-\lambda^w - h\right)\right] \quad \text{Eq. 4}$$

$$\pi_4 = 1 - \exp\left[-\exp\left(\lambda^w + h\right)\right] \quad \text{Eq. 5}$$

$$\pi_5 = 1 - \frac{1}{1 + \lambda^{w+\lambda \cdot h}} \quad \text{Eq. 6}$$

where P_o, P_1, w and h are the four parameters of the probability distributions. Each theoretical distribution is fitted to the empirical cumulative probability using a Newton-type algorithm (Dennis and Schnabel, 1983). In order to obtain a better correspondence between precipitation and return period, the mean square error was minimized not only for the low cumulative probability but also for the high (symmetrical weighting for the lowest and highest values), thus the measure to minimize is a dual mean normalized square error (DNSE):

$$DNSE = \frac{1}{N}\sum_{i=1}^{N} \frac{\left(\pi_{k,i} - \pi_{emp,i}\right)^2}{\pi_{emp,i}^{\ 2}} \cdot \frac{\left[\left(\pi_{k,i} - 1\right) - \left(\pi_{emp,i} - 1\right)\right]^2}{\left(\pi_{emp,i} - 1\right)^2} \quad \text{Eq. 7}$$

where the first and second factors of the product are respectively for low and high cumulative probability. All the fits were carried out using a parametric initialization obtained by maximum likelihood inference (Coles, 2001, Raue *et al.*, 2009). Inference with Profile Log-Likelihood approach was applied to the CDF (see appendix A).

3.3 Return periods estimation

The return period, y, of a precipitation higher than p is defined as the inverse of the probability of a rainfall higher than p is recorded in one day, i.e., $y(p) = 1/[1-\pi(p)]$, where $\pi(p)$ is the value of the ECDF or TCDF for a precipitation p. To estimate precipitations associated with certain return periods, we used theoretical probability distributions (π_k). Each theoretical probability (Eq. 2 to 6) is fitted to the empirical cumulative probability (π_{emp}). Finally, the expected precipitation p of a certain return period of interest y is given as:

$$p(y) = \frac{1}{\sum_j \frac{1}{MNAE_j^{\ 2}}} \sum_k \frac{\pi_k^{\ -1}(y)}{MNAE_k^{\ 2}} \quad \text{Eq. 8}$$

where π_k^{-1} is the inverse function of the k-distribution, y is the cumulative probability corresponding to the return period of interest, and $MNAE_k$ is the mean normalized absolute error of the k-distribution, i.e.:

$$MNAE_k = \frac{1}{n}\sum_{i=1}^{n} \left| \frac{p_{i,k} - p_{i,emp}}{p_{i,emp}} \right| \quad \text{Eq. 9}$$

where $p_{i,emp}$ is the empirical precipitation greater than 0 corresponding to each i-value of the empirical cumulative probability (π_{emp}); $p_{i,k}$ is the corresponding fitted i-value, according to the theoretical k-distribution (π_k). Finally, n is the number of different values of precipitation greater than 0, according to the empirical cumulative probability. To validate the simulation of the extreme values, the last two values of the tail are not used for the fits.

3.4 Systematic error correction

A systematic error is obtained by comparing the simulated precipitation (from climate models *historical experiment*) with the observed precipitation (from reference time-series). In order to correct this systematic error, it is necessary to have long time-series of reference, because the large natural variability of precipitation has a significant uncertainty associated. For that reason, we have extended the observed time series downscaling ERA40 reanalysis (1958-2000) before validation. Due to systematic error that downscaling method introduces into the extreme rainfall, we chose to correct the ECDF of each ERA40 simulation (p_{era}), with reference to observations (p_{obs}) in the common period (marked as *). This correction is based on quantile-quantile parametric transferences (Benestad, 2010, Monjo *et al.*, 2014). Therefore, the extended time-series (p_{obs}') of each rain gauge is:

$$p_{obs}' = p_{obs} \cup \pi_{obs*}^{-1}\left(\pi_{era*}(p_{era})\right) \quad \text{Eq. 10}$$

where π_{obs*} and π_{era*} are the ECDFs of the observed rainfall and of the downscaled ERA40 simulation, estimated in the common period. The symbol $\cup$ joins two time-series: the term on the right is the result of the correction of downscaled ERA40 rainfall, while the term on the left is the original observed time-series (p_{obs}).

After obtaining the extended time-series (p_{obs}'), the same probabilistic correction was applied for the downscaled projections simulated by the climate models (CMs), according to:

$$p_{CM}' = \pi_{obs'*}^{-1}\left(\pi_{CM*}(p_{CM})\right) \quad \text{Eq. 11}$$

where π_{CM*} is the ECDF of the downscaled CM simulation, estimated in the common period with the extended time-series, and $\pi_{obs'*}$ is the ECDF of this extended observed time-series (p_{obs}').

3.5 Statistical analysis

First, we analyzed the goodness of the process of extending each time series using the ERA40 reanalysis. For this, the mean normalized absolute error (MNAE) is obtained for the five probability distributions fitted to the time-series pairs (observed and simulated). In addition, the Kolmogorov-Smirnov test (Marsaglia *et al.*, 2003) was applied to analyse the statistical significance of the similarity of the time-series after probabilistic correction.

For analysis of extreme rainfall, four different return periods are considered: 10, 20, 50, and 100 years. A validation of the method is done by comparing the downscaled ERA40 simulation with the observed time-series. The comparison is performed before and after applying the probabilistic correction, in the common period for each station, and for each return period. Similarly, extreme precipitation obtained for *historical* simulation of the models is compared with the extended observed series.

To analyze the possible change of extreme precipitation, the reference period was considered as large as possible (50 years), i.e. 1951-2000 for the past and 2051-2100 for the future. The significance of the change is estimated for the RCP4.5 and RCP8.5 scenarios, with a p-value for the whole of the 9 climate models, by using the Kolmogorov-Smirnov test (KS) and the Student's t-test (ST). All p-values were calculated assuming independence between the time-series.

4 Results

4.1 Validation of the method for extreme precipitation

For extending each observed time-series, it was found that simulation obtained by downscaling ERA40 (output) is climatically very similar to the observed time-series used as base (input). In particular, the simulated time-series passed the Kolmogorov-Smirnov test (p-value > 0.05, comparing with the observations) for general rainfall. However, the test was not passed for the most intense rainfall (e.g. with return period greater than 1 year). This result justified the need to

correct the simulated time-series to extend time-series, and to study the extreme rainfall of all simulations. Alternatively, relations with the closest and longest observations were explored, but finally they were not used for extending because are generally less similar to each observed series than its simulation from the downscaled ERA40.

In order to prepare the correction, theoretical distributions were weighed according its MNAE of fit, separately for observed and simulated time-series. The best distributions were generally different for the observed time-series and for the simulated ones, moreover, the first were fitted with a lower error (Fig. 2). Modified Log-Logistic was chosen more times (as the best fit) for the observed data, while for the simulated data the Reversed Gumbel was obtained more times. In any case, the best fit for each time-series presented a MNAE between 0.02 and 0.12 for the observations and between 0.02 and 0.22 for simulations of downscaled ERA40 (Fig. 2, black boxplot). This goodness-of-fit was considered enough to apply a probabilistic correction to the simulated series using the best transfer function in each case.

However, the fit prediction of the two highest values of each distribution shows a MNAE between 0.05 and 0.26 for the most of the rain gauges, particularly between the first (Q1) and third (Q3) quartiles of the cases (for both observations and simulations). In cases with worse ranking (e.g. 90^{th} percentile of the worst rain-gauges), the MNAE is greater than 0.5. This result shows the limitation and the high uncertainly linked to the natural variability of the most extreme precipitation.

For this reason, a comparative analysis of the extremes was carried out before and after correcting the simulated time-series, for the common period of observations. Before probabilistic correction, the ERA40 extreme precipitation (simulated by downscaling) had a bias between –12 and –40% for a 10y-return and –50 and –20% for a 100y-return, for its Q1 and Q3 (Fig. 3, right). After correction, the bias decreased and placed generally between –12 and +12%, and simulations passed the Kolmogorov-Smirnov (p-value > 0.05) for the extreme rainfall, comparing with the observations. Therefore, the method was validated for our purpose and can be applied to remaining steps of study.

Each observed time-series were extended using its associated simulation of downscaled ERA40, after correction; and with these extended series, the climate projections of the CMs also were corrected. The bias of the extreme precipitation, obtained for the *historical* simulation of the models, is also about between –12 and +12% (Q1 and Q3) when compared to the extended observations in the common period (Fig. 4, right). With this, the mean absolute error of the 100y-return precipitation simulated by the *historical* is mainly between 5 and 25%. This result is similar to the MNAE of highest values obtained by fitting the theoretical distributions to the observations. Combining the nine climate models, final error for the extreme precipitation estimation is about ±7% (Q1 and Q3) with a MNAE between 3 and 15%. Therefore, this range error is obtained from the limitation of the used methodology.

4.2 Projected changes in extreme precipitation

Projections showed a general decrease in annual mean precipitation (changes between –7% of Q1 and –20% of Q3), which are in agreement with other studies (Collins *et al.*, 2013). However, the decrease is less clear when we focus on the most intense precipitation. For example, slight changes in the 95^{th} percentile are expected between –3% and –6% (Q1 and Q3) for most of studied stations. Possible changes in the extreme precipitation are mainly between –20% and +15% for the 10y-return period, and between –25% and +25% for the 100y-return period, according to both RCP4.5 and RCP8.5 scenarios. Significance in the changes was analysed using the ensemble strategy.

In most of the cases, random errors (from section 4.1) are too large compared to the changes of extreme precipitation estimated by the climate projections. The use of ensembles of models can help to better quantify the uncertainty associated with the natural variability of extreme precipitation.

In fact, after conducting an ensemble analysis, some stations show significant changes for the 10y-return precipitation, with decreases of between 10 and 30%. In particular, these are three for the RCP4.5 (Fig 5 left) and six stations for the RCP8.5 (Fig. 5 right). For the other studied return periods, the projected changes are similar –the decreases predominate over the possible increases. This predominance is somewhat lower for the 100y-return precipitation (Fig. 6): only one station for RCP4.5 and three for RCP8.5 show decreases with a significance level (p-value > 0.9). Higher decreasing in low intensities is also found by Rajczak *et al.* (2013) for the Mediterranean basin, according with several regional climate models from the ENSEMBLES project (van der Linden and Mitchell, 2009). However, the same models projected that Mediterranean will experience an increase in heavy precipitation (Rajczak *et al.*, 2013).

In the present study, a statistically non-significant increase greater than 20% is projected under both scenarios for the 100y-return precipitation in the coastline of southern Valencia and northern Alicante. This possible increase (p-value > 0.5) would be expected close to the station where the maximum precipitation was recorded (see Fig. 1). In that area, extreme rainfall could suffer a certain displacement towards the sea; i.e., results show a possible decrease in a few kilometers inland but with a possible increase in the coastline. Although there are some differences in magnitude between the two scenarios, a spatial consistence (between inland and coastline) is observed for the sign of the possible change in that region. Projected relative changes are similar (in terms of sign and value) for the 50y-return precipitation but with a lower significance; therefore only the 100y-return is shown. The 20y-return precipitation is projected with an intermediate change in magnitude respect to the 10 and the 100y-return period. These results are consistent with the Fifth Assessment Report of the IPCC, which does not project significant changes in 20y-return rainfall for the study area (Collins *et al.*, 2013).

In most of the cases, some random differences in magnitude and significance of the projected changes can be found between the RCP4.5 and RCP8.5 scenarios, but no general differences in the sign of the possible changes. For example, for the 10y-return precipitation, when the significance level is reached under a scenario, it is not achieved (but is generally close) in the same locations for the other one. The differences can be explained as a consequence of the non-linear behaviour of precipitation, as well as of its natural variability. In other words, although *a priori* more significant changes could be expected under the RCP8.5, they can be diluted by the natural cycles and even smoothed by a non-linear compensating mechanism regarding a minor radiative forcing (e.g. under the RCP4.5) (Mitchell and Hulme, 1999). Finally, an alternative or complementary explanation is to assume that natural variability of precipitation is possibly greater than the climate response to radiative forcings in the studied area (see section 5.2).

5 Discussion

5.1 Choice of climate predictors

Selection of climate predictors should be carried out based on theoretical considerations and the final use of the downscaled simulation. In particular, three basic ideas were considered in the used downscaling method:

1. The stationarity: The physical forcings of the selected predictands should be strongly linked to the predictands in order to these linkages do not change. In contrast, the use of empirical analyses could result in non-physically based relationships that may be not applicable in the future due to the stationarity problem.

2. The no seasonality: Since the climatic characteristics of the calendar seasons may change, predictors/predictands relationships detected in a particular season of the "present climate" would not be applicable for the future climate. In fact, seasonal stratification does not improve the skill of the used method, hopefully because the relationships it uses correctly reflect the

physical links between predictors and predictands, i.e., they are not just empirical relationships (Ribalaygua *et al.*, 2012).

3. The limitations of the GCMs: Due to the method is finally applied to GCM outputs, predictors selected should be well simulated by the GCMs. According to this, some general and theoretical considerations have been identified:

- The predictors should be relative and field variables, rather than absolute and point values, because the former are more reliably simulated by GCMs.
- The predictors should be suitable for the available temporal and spatial resolution of the GCM outputs. Many of the physical forcings of the predictands can only be captured working at temporal and spatial scales that are as small as possible. This could be especially relevant for the simulation of some extreme precipitation events. For these reasons, we work at daily and synoptic scales, because these are the scales at which the GCMs provide better information.
- The predictors should be easily resolved by the models. For example, GCMs simulate better free-atmosphere rather than boundary layer variables. Geostrophic winds are some of the variables best simulated (Brands *et al.*, 2010). Moisture fields are not considered in this work because some GCMs present difficulties to simulate (Hu *et al.*, 2005; John and Soden 2007; Brands *et al.*, 2010).

With all these ideas, geostrophic winds at 1000 and 500hPa were selected as representatives of atmospheric configuration. Other important predictors, such as the moisture, have been left out. However, if moisture captures physical links for precipitation, these are related with the forcings by upwards movements of air. In fact, the most important forcings of upward movements are three: (1) dynamic forcing, (2) topographic lift and (3) convection.

Dynamic forcing at synoptic scale is determined by geopotencial configurations at 1000 and 500 hPa. Topographic lift could be considered attending at surface winds, which are strongly related to geostrophic flux at 1000 hPa.

Convection is an upward movement caused by sensible and latent heats. Due to the small scale of this phenomenon in its initial state, this is the most difficult upward movement forcing to simulate. However, we can assume that synoptic configuration (mainly 500 and 1000 hPa) determines both the presence of necessary moisture (e.g. by wind direction) and the presence of unstable atmospheric profile (thermal or dynamic instability) for the convection occurrence: presence of "heat lows" and/or depressions at high levels. However, this approach shows some limitations because other triggering factors are also necessary (differential surface heating, breeze/wind, topographic lifts, frontal lifts, gust front of other storms, etc.).

5.2 Cascade of uncertainty

Final projections have an important uncertainty which is the sum of the four main sources: (1) downscaling/correction methodology, (2) CMIP5 climate models / runs, (3) choice of RCP scenarios and (4) natural variability of precipitation (e.g. interannual variation).

The choice of downscaling methodology is a key to achieve climate simulations consistent with observations and which in turn are physically robust. The analogue stratification reflects the non-linear physical connection between a certain synoptic configuration and the local precipitation. We assume that although the frequency of each synoptic configuration will change, its physical connection will be similar to the past (stationarity). This can be observed in the ability of the method to reproduce the evolution of the recent climate (Ribalaygua *et al.*, 2012).

The used statistical downscaling method has been compared with other statistical and dynamical downscaling methods, obtaining good results for Spain and Europe (STARDEX 2005, van der Linden and Mitchell 2009, Goodess *et al.* 2011). Nevertheless, the method still has limitations to simulate the most extreme precipitation, and therefore requires a correction of systematic error. The final bias of the corrected simulation is a random error between –12 and +12% (Q1 and Q3), which is low for a variable as the extreme precipitation. This may be due to

the novel correction method, which uses theoretical distributions that fits the entire probability curve, not just the upper tail. For this reason, classical 3-parametric distributions as LogNormal and Generalized Extreme Value cannot be considered in this study (Moncho *et al.* 2012).

All fits are performed using the whole ECDF because the estimation of return periods has a great sensitivity depending on the number of available values of precipitation (i.e., length of time-series). That is, fit is better (less over-fitting) when all points of an ECDF are considered, in contrast to when only values exceeding a threshold are taken into account. However, an important uncertainty is expected when a fitted CDF is extrapolated for return periods very higher than length of time-series (e.g. 100y-return). In order to reduce the extrapolation error, five theoretical CDFs have been used (Eq. 2-6). The comparison between final simulations and observations for high return periods (Fig. 3) shows a low error (about 10%) for the extrapolated values, which guarantee the coherence of the extrapolation method.

In other hand, an ensemble strategy with nine models was used to reduce the uncertainty associated with climate models. Combining the nine climate model outputs, final methodological error for the extreme precipitation estimation is about ±7%. However it seems that natural variability achieves mask changes in extreme precipitation projected by models. That is, possible changes between -30 and 30% are less than the interannual and interdecadal variability. In fact, the differences between the used RCP scenarios do not follow a pattern consistent with a progressive climate response to radiative forcing. That is, the projected changes are not substantially greater for the higher RCP.

Interpretation of the results presents an additional constraint. The non-significant variation of extreme precipitation should be understood mainly in terms of the frequency of occurrence. That is, the statistical downscaling method is used to capture synoptic configurations that cause extreme rainfall, and thus, changes in frequency of these configurations are reflected by the climate projections. However, the non-significance of the projected variations does not take into account directly the possible effect of increased precipitable water due to global warming (Wang *et al.*, 2008, Ye *et al.*, 2014). Despite this, an increase of wettest configurations could be indirectly captured by the analogue stratification in the climate projections. These possible effects will be explored in future works considering several issues: 1) the incorporation of new predictors in the analogue stratification tends to smooth the distribution of the similarity measure; 2) for extreme rainfall events, the occurrence depends more on an infrequent synoptic configuration (500hPa/1000hPa) than on the precipitable water; 3) when the event occurs, precipitable water influences on the final rainfall amount.

6 Conclusions

The methodology used to calculate the extreme precipitation has a significant advantage over classical methods of fitting probability distribution. The five used theoretical distributions adequately fit to the entire empirical curve. Therefore, the combination of these curves is able to reduce the estimation error of extreme rainfall, avoiding overshooting in the upper tail. The best fit for each time series presented a mean normalized absolute error between 0.05 and 0.28 (Q1 – Q3). The final error of the extreme precipitation estimation was between –12 and +12% (Q1 and Q3), for each climate simulation. With this, the eighteen analyzed projections show that changes in extreme rainfall patterns generally be non-significant compared with the natural variability of precipitation. However, for some places, significant changes are detected in the extreme rainfall for the 2051-2100 when comparing with the 1951-2000 period. Maximum 24h rainfall could decrease about 20% in some areas during the common *cut-off low* episodes (10y-return), but not for the most extreme *cut-off low* episodes (100y-return). In fact, a possible increase about 20% is projected under both scenarios for the 100y-return precipitation in the coastline of southern Valencia and northern Alicante. In this area, extreme rainfall could suffer a certain displacement towards the sea.

In general, some random differences in the magnitude and significance of the projected changes can be found between the RCP4.5 and RCP8.5 scenarios, but no differences in the sign. This is probably due to the large interdecadal variability, which achieves to mask the significance of climate change. Nevertheless, these results should be interpreted with caution because of the limited number of models and climate scenarios. This work shows that the developed methodology is useful for studying extreme rainfall under different climate scenarios. However, the study shows several improvable issues such as the possible incorporation of the precipitable water in the second step of the method (section 3.1) and application to a larger number of climate projections.

6 Acknowledgments

The authors thank the Spanish Meteorology Agency (Agencia Estatal de Meteorología – AEMet) for providing the observed data set and the European Centre for Medium-Range Weather Forecasts (ECMWF) for offering the ERA-40 reanalysis data (http://data-portal.ecmwf.int/data/d/era40_daily). We also acknowledge the World Climate Research Programme's Working Group on Coupled Modelling, which is responsible for CMIP, and we thank the climate modelling groups (listed in Table 1 of this paper) for producing and making available their model output.

Appendix A. Mathematical considerations

A.1 Used log-likelihood function

Density probability of the empirical values of precipitation has not sense. That is, due to the limited resolution data (usually 0.1 mm), measured values are discrete with repetitions. Therefore, cumulative distribution function (CDF, π) and the empirical CDF (ECDF, π_{emp}) are taken to analyze the likelihood. Given a theoretical CDF, $\pi(x_i, p)$, with k parameters $p = (p_1, p_2, \ldots, p_k)$, and assuming independent values of precipitation x_i, the likelihood L can be defined as (Owen, 2001):

$$L \equiv \prod_{i=1}^{n} \left(\pi(x_i, p) - \pi(x_{i-1}, p)\right)^{y_i} \qquad \text{Eq. A1}$$

where y_i is the absolute frequency of each one of the n different values of precipitation x_i, sorted from the lowest to the highest. For precipitation less than zero, $x_0 < x_1 = 0$, it is taken $\pi(x_0) \equiv 0 \equiv \pi_{emp}(x_0)$. Therefore, the log-likelihood function is:

$$\ln L = \sum_{i=1}^{n} y_i \ln\left(\pi(x_i, p) - \pi(x_{i-1}, p)\right) \qquad \text{Eq. A2}$$

The absolute frequency y_i can be written as:

$$y_i = N \cdot \left(\pi_{emp}(x_j) - \pi_{emp}(x_{j-1})\right) \qquad \text{Eq. A3}$$

Then, log-likelihood is:

$$\ln L = N \sum_{i=1}^{n} \left(\pi_{emp}(x_i) - \pi_{emp}(x_{i-1})\right) \ln\left(\pi(x_i, p) - \pi(x_{i-1}, p)\right) \qquad \text{Eq. A4}$$

A.2 Critical issues for extreme values

The maximization of the log-likelihood is dominated by the most frequent values (approximately for $\pi < 0.75$). Hence, fit is not optimized for the highest values of the precipitation. Alternatively, the fit can be restricted to only high values, according to the extreme value theory (Coles, 2001). In accordance with the extremal type theorem, the expected distribution is a Gumbel (type I, Eq. A5), Fréchet (type II, Eq. A6) or Reversed Weibull (type III Eq. A7).

$$\pi_G = \exp\left[-\exp\left(-\lambda\right)\right] \quad \text{Eq. A5}$$

$$\pi_F = \exp\left[-\lambda^{-w}\right] \quad \text{Eq. A6}$$

$$\pi_W = \exp\left[-\left(-\lambda\right)^{w}\right] \quad \text{Eq. A7}$$

with w taken as shape parameter and λ defined as:

$$\lambda(p; P_o, P_1) \equiv \frac{p - P_o}{P_1} \quad \text{Eq. A8}$$

where p is the daily precipitation, parameter P_o is the most probable value and P_1 is the scale factor.

The type III can be rewritten for the negative of the precipitation because Reversed Weibull is truncated for a positive value (in contrast with the observed precipitation). The Fréchet can be approximated by Taylor for extreme values $\lambda >> 1$ as:

$$\pi_F = \frac{1}{\exp\left(\frac{1}{\lambda^w}\right)} \approx \frac{1}{1+\frac{1}{\lambda^w}} = \frac{\lambda^w}{1+\lambda^w} \quad \text{Eq. A9}$$

However, several problems are raised. Usually, extreme values of precipitation are taken as the maximum daily amount of each year to build a full data set. Nevertheless, some daily values of a same year can be more extreme than the maximum value of other years. For this reason, a better estimation of return periods is achieved if all daily values are taken. With this assumption, it is necessary to define the beginning of the extreme tail by a cut-off threshold. Although we are interested in rainfall of very high return periods (especially 100 years), the available data are usually about 10 or 20 years in length. How many values of the tail must be taken to fit some extreme type distribution? The arbitrariness of selecting a cutting value can affect the outcome, especially since the maximum likelihood fitting heavier for the most frequent (low) values. In addition, if a few values of the tail are taken then it is very likely that the fit suffers overfitting. Therefore, this paper search alternatives that attempt to address these issues (avoiding cut-offs and overfitting, while respecting the extreme tail satisfies the extreme value theory).

A.3 Proposed solution

In order to solve the above problems, it is suggested to use theoretical CDFs attempting to be fitted to whole ECDF. These CDFs must satisfy its tail tends to resemble some type of extreme-value distribution. Particularly, in the limit as $\lambda^w >> h$ three of our distributions tend to resemble type I (Gumbel) or the rewritten type III (Weibull):

$$\pi_2 = 1 - \exp\left(-\lambda^w - h\right) \;\rightarrow\; \pi_2 \approx 1 - \exp\left(-\lambda^w\right) \quad \text{Eq. A10}$$

$$\pi_3 = \exp\left[-\exp\left(-\lambda^w - h\right)\right] \;\rightarrow\; \pi_3 \approx \exp\left[-\exp\left(-\lambda^w\right)\right] \quad \text{Eq. A11}$$

$$\pi_4 = 1 - \exp\left[-\exp\left(\lambda^w + h\right)\right] \;\rightarrow\; \pi_4 \approx 1 - \exp\left[-\exp\left(\lambda^w\right)\right] \quad \text{Eq. A12}$$

The Fréchet type can be found for $h << w/\lambda$:

$$\pi_5 = 1 - \frac{1}{1+\lambda^{w+\lambda \cdot h}} \;\rightarrow\; \pi_5 \approx \frac{\lambda^w}{1+\lambda^w} \quad \text{Eq. A13}$$

Choosing $h \approx 1$, gamma distribution is the rewritten type III:

$$\pi_1 = \frac{\gamma\left(h, \lambda^w\right)}{\Gamma\left(h\right)} \;\rightarrow\; \pi_1 \approx 1 - \exp\left(-\lambda^w\right) \quad \text{Eq. A14}$$

Therefore, our distributions include the three types of extreme-value distributions, at least for the tails or for a particular value of h. With this, there is an additional degree of freedom, h, which is intended to serve as a bridge between the shape of the distribution for the low values and the shape of the curve for the high values. Thereby, the transition between non-extreme and extreme values is smoother, decreasing the effect of overfitting.

In other hand, the maximization of the log-likelihood is very useful to found of value of h and P_o, since they are related with the most frequent values of precipitation. However, the fit of w and P_1 require a special approach which is to minimize the dual mean normalized square error (DNSE):

$$DNSE \equiv \frac{1}{N}\sum_{i=1}^{N}\frac{\left(\pi_{k,i}-\pi_{emp,i}\right)^2}{\pi_{emp,i}{}^2}\cdot\frac{\left[\left(\pi_{k,i}-1\right)-\left(\pi_{emp,i}-1\right)\right]^2}{\left(\pi_{emp,i}-1\right)^2} \qquad \text{Eq. A15}$$

where the first and second factors of the product are respectively for low and high cumulative probability. This minimization allows fitting 4-parametric distributions to whole ECDF of daily precipitation.

Note that DNSE uses a symmetrical weighting for the lowest and highest values of precipitation, in contrast with the classic normalized square error (NSE). If one minimizes the NSE of the CDF, the result is over-fitted on the bottom of the CDF (because the top is saturated to 1). In a similar way, if one minimizes the NSE of the complementary curve (1 – CDF), the result is over-fitted on the top of the CDF. DNSE is defined as the product of both errors, so a symmetrical weighting is achieved for the bottom and top of the CDF.

References

AEMet (2007) *Resumen de extremos climatológicos en España*. Spanish Meteorological Agency http://www.aemet.es/documentos/es/divulgacion/resumen_efemerides/Resumen_extremos.pdf News release: http://www.levante-emv.com/portada/3747/reconocen-record-diluvio-oliva/380968.html. (Last access 1th September 2014)

Armengot-Serrano R. 1994. Las precipitaciones extraordinarias. In: Pérez Cueva, A. (Ed.) *Atlas climàtic de la Comunitat Valenciana*. Conselleria d'Obres Públiques, Urbanisme i Transports. Generalitat Valenciana, Spain. *Col·lecció Territori* **4**: 98-99. ISBN: 84-482-0309-7.

Benestad RE. 2010. Downscaling precipitation extremes. Correction of analog models through PDF predictions. *Theoretical and Applied Climatolology* **100**: 1–21.

Bentsen M, Bethke I, Debernard JB, Iversen T, Kirkevåg A, Seland Ø, Drange H, Roelandt C, Seierstad IA, Hoose C, Kristjánsson, JE. 2012. The Norwegian Earth System Model, NorESM1-M – Part 1: Description and basic evaluation. *Geoscientific Model Development Discussion* **5**: 2843-2931. doi:10.5194/gmdd-5-2843-2012.

Brands S, Herrera S, San-Martin D, Gutierrez JM. 2011. Validation of the ENSEMBLES global climate models over southwestern Europe using probability density functions, from a downscaling perspective. Climate Research **48**:145–161. doi:10.3354/cr00995.

Capel-Molina JJ. 2000. *El Clima de la Península Ibérica*. Ed. Ariel, Barcelona, Spain. ISBN: 84-344-3466-0.

Chylek P, Li J, Dubey MK, Wang M, Lesins G. 2001. Observed and model simulated 20th century Arctic temperature variability: Canadian Earth System Model CanESM2. Atmos Chem Phys Discuss **1**1: 22893-22907, doi:10.5194/acpd-11-22893-2011.

Coles, E. 2001. An Introduction to Statistical Modeling of Extreme Values. Springer, London, UK. ISBN: 1-85233-459-2.

Collins WJ, Bellouin N, Doutriaux-Boucher M, Gedney N, Hinton T, Jones CD, Liddicoat S, Martin G, O'Connor F, Rae J, Senior C, Totterdell I, Woodward S, Reichler T, Kim J, Halloran P. 2008. Evaluation of the HadGEM2 model. Hadley Centre Technical Note HCTN 74, Met Office Hadley Centre, Exeter, UK.

Collins M, Knutti R, Arblaster J, Dufresne JL, Fichefet T, Friedlingstein P, Gao X, Gutowski WJ, Johns T, Krinner G, Shongwe M, Tebaldi C, Weaver A,Wehner M. 2013. Long-term climate change: projections, commitments and irreversibility. In: *Climate Change 2013: The Physical Science Basis. Contribution of Working Group I to the Fifth Assessment Report of the*

Intergovernmental Panel on Climate Change [Stocker TF, Qin D, Plattner GK, Tignor M, Allen SK, Boschung J, Nauels A, Xia Y, Bex V, Midgley PM (eds.)]. Cambridge University Press, Cambridge, UK and New York, NY, USA. doi:10.1017/CBO9781107415324.

Dennis, J. E. and Schnabel, R. B. (1983) Numerical Methods for Unconstrained Optimization and Nonlinear Equations. Prentice-Hall, Englewood Cliffs, NJ.

Dunne JP, John JG, Adcroft AJ, Griffies SM, Hallberg RW, Shevliakova E, Stouffer RJ, Cooke W, Dunne KA, Harrison MJ, Krasting JP, Malyshev SL, Milly PCD, Phillipps PJ, Sentman LT, Samuels BL, Spelman MJ, Winton M, Wittenberg AT, Zadeh N. 2012. GFDL's ESM2 Global Coupled Climate–Carbon Earth System Models. Part I: Physical Formulation and Baseline Simulation Characteristics. *Journal of Climate* **25**: 6646–6665. doi:10.1175/JCLI-D-11-00560.1.

Egozcue JJ, Ramis C. 2001. Bayesian hazard analysis of heavy precipitation in eastern Spain. *International Journal of Climatology* **21**: 1263-1279.

Font-Tullot I. 2000. *Climatología de España y Portugal*, Universidad de Salamanca, Spain. ISBN: 84-7800-944-2.

Gil A, Olcina J. 1999. *Climatología Básica.* Ariel, Colección Geografía. Barcelona, Spain. ISBN: 84-344-3462-8.

Goodess CM, Anagnostopoulou C, Bárdossy A, Frei C, Harpham C, Haylock MR, Hundecha Y, Maheras P, Ribalaygua J, Schmidli, J., Schmith T, Tolika K, Tomozeiu R, Wilby RL. 2011. *An intercomparison of statistical downscaling methods for Europe and European regions – assessing their performance with respect to extreme temperature and precipitation events*. Climate Research Unit Research Publication (CRURP) N.11, University of East Anglia, UK, [http://www.cru.uea.ac.uk/cru/pubs/crurp/CRU_RP11.pdf]

Herrmann JM. 2008. Relevance of ERA40 dynamical downscaling for modeling deep convection in the Mediterranean Sea. *Geophysical Research Letters* **35**: L04607. doi:10.1029/2007GL032442.

Hu H, Oglesby RJ, Marshall S. 2005. The simulation of moisture processes in climate models and climate sensitivity. Journal of Climate **18**:2172–2193. doi: 10.1175/JCLI3384.1

Imbert A, Benestad R. 2005. An improvement of analog model strategy for more reliable local climate change scenarios. Theor Appl Climatol 82:245–255. doi: 10.1007/s00704-005-0133-4

Iversen T, Bentsen M, Bethke I, Debernard JB, Kirkevåg A, Seland Ø, Drange H, Kristjánsson JE, Medhaug I, Sand M, Seierstad IA (2012) The Norwegian Earth System Model, NorESM1-M – Part 2: Climate response and scenario projections. Geosci Model Dev Discuss 5: 2933-2998. doi:10.5194/gmdd-5-2933-2012.

John VO, Soden BJ. 2007. Temperature and humidity biases in global climate models and their impact on climate feedbacks. Geophysical Research Letters **34**:L18704. doi:10.1029/2007GL030429

Lazier JR, Pickart RS, Rhines PB. 2001. Deep convection. In: Lazier JR (ed) Ocean circulation and climate. Observing and modelling the global ocean. Academic Press, London, UK.

Llasat MC, Ramis C, Barrantes J. 1996. The meteorology of high-intensity rainfall events over the West Mediterranean region. *Remote Sensing Reviews* **14**: 51–90. doi:10.1080/02757259609532313.

Marsaglia G, Tsang WW, Wang J. 2003. Evaluating Kolmogorov's distribution, J Stat Software 8: 18.

Marsland SJ, Haak H, Jungclaus JH, Latif M, Roeske F. 2003. The Max-Planck-Institute global ocean/sea ice model with orthogonal curvilinear coordinates. Ocean Modelling **5**: 91-127. doi: 10.1016/S1463-5003(02)00015-X.

Martín-Vide J, Olcina J. 2001. *Climas y tiempos de España*, Madrid, Alianza Editorial. ISBN: 84-206-5777-8

Martín-Vide J. 2004. Spatial distribution of a daily precipitation concentration index in peninsular Spain. *International Journal of Climatology* **24**: 959-971.

Mitchell TD, Hulme M (1999): Predicting regional climate change: living with uncertainty, Prog. Phys. Geog 23: 57–78.

Moncho R, Caselles V, Chust G. 2012. Alternative model for precipitation probability distribution: application to Spain. *Climate Research* **51**: 23-33, doi: 10.3354/cr01055.

Monjo R, Caselles V, Chust G. 2014. Probabilistic correction of RCM precipitation in the Basque Country (Northern Spain). *Theoretical and Applied Climatology* **117**: 317-329. DOI: 10.1007/s00704-013-1008-8.

Owen, A. B. 2001. Empirical likelihood. CRC Press LLC, London, UK. ISBN 1-58488-071-6.

Pérez-Cueva A (1983) Precipitaciones extraordinarias en la España Peninsular. *Agricultura y sociedad*, **28**: 189–203. ISSN: 0211–8394.

Raddatz TJ, Reick CH, Knorr W, Kattge J, Roeckner E, Schnur R, Schnitzler K-G, Wetzel P, Jungclaus J. 2007. Will the tropical land biosphere dominate the climate-carbon cycle feedback during the twenty first century?. *Climate Dynamics* **29**: 565-574. doi: 10.1007/s00382-007-0247-8.

Rajczak J, Pall P, Schär C. 2013. Projections of extreme precipitation events in regional climate simulations for Europe and the Alpine Region. *Journal of Geophysical Research: Atmospheres* **118**: 2169-8996. doi: 10.1002/jgrd.50297

Ramis C, Homar V, Amengual A, Romero R, Alonso S. 2013. Daily precipitation records over mainland Spain and the Balearic Islands. *Natural Hazards and Earth System Sciences* **13**: 2483–2491. doi:10.5194/nhess-13-2483-2013.

Raue A, Kreutz C, Maiwald T, Bachmann J, Schilling M, Klingmüller U, Timmer J. 2009. Structural and practical identifiability analysis of partially observed dynamical models by exploiting the profile likelihood. *Bioinformatics* **25**: 1923–9.

Ribalaygua J, Torres L, Pórtoles J, Monjo R, Gaitán E, Pino MR. 2012. Description and validation of a two-step analogue/regression downscaling method. *Theoretical and Applied Climatology* **114**: 253-269. doi:10.1007/s00704-013-0836-x.

STARDEX, 2005. *STARDEX Final Report- Downscaling Climate Exremes*, European Union. http://www.cru.uea.ac.uk/projects/stardex/reports/STARDEX_FINAL_REPORT.pdf

Taylor KE, Stouffer RJ, Meehl GA. 2009. *A summary of the CMIP5 experiment design*. PCDMI Rep. Available in http://cmip-pcmdi.llnl.gov/cmip5/docs/Taylor_CMIP5_design.pdf (Last access 1th September 2014).

Taylor KE, Stouffer RJ, Meehl GA. 2012. An overview of CMIP5 and the experiment design. *Bulletin of the American Meteorological Society* **93**: 485–498. doi:10.1175/BAMS-D-11-00094.1.

Uppala SM, KÅllberg PW, Simmons AJ, Andrae U, Bechtold VDC, Fiorino M, Gibson JK, Haseler J, Hernandez A, Kelly GA, Li X, Onogi K, Saarinen S, Sokka N, Allan RP, Andersson E, Arpe K, Balmaseda MA, Beljaars ACM, Berg LVD, Bidlot J, Bormann N, Caires S, Chevallier F, Dethof A, Dragosavac M, Fisher M, Fuentes M, Hagemann S, Hólm E, Hoskins BJ, Isaksen L, Janssen PAEM, Jenne R, Mcnally AP, Mahfouf J.-F, Morcrette J.-J, Rayner NA, Saunders RW, Simon P, Sterl A, Trenberth KE, Untch A, Vasiljevic D, Viterbo P and Woollen J. 2005. The ERA-40 re-analysis. *Quarterly Journal of the Royal Meteorological Society* **131**: 2961–3012. doi:10.1256/qj.04.176. Data Source (online) available in: http://www.ecmwf.int/research/era/do/get/era-40 (Last access 1th September 2014).

van der Linden P, Mitchell JFB (eds.) 2009: *ENSEMBLES: Climate Change and its Impacts: Summary of research and results from the ENSEMBLES project.* Met Office Hadley Centre, UK. 160pp. http://ensembles-eu.metoffice.com/docs/Ensembles_final_report_Nov09.pdf (see. p 68) (Last access 1th September 2014).

Voldoire A, Sanchez-Gomez E, Salas y Mélia D, Decharme B, Cassou C, Sénési S, Valcke S, Beau I, Alias A, Chevallier M, Déqué M, Deshayes J, Douville H, Fernandez E, Madec G, Maisonnave E, Moine M-P, Planton S, Saint-Martin D, Szopa S, Tyteca S, Alkama R, Belamari S, Braun A, Coquart L, and Chauvin F. 2013. The CNRM-CM5.1 global climate

model: description and basic evaluation, *Climate Dynamics* **40**: 2091-2121, doi: 10.1007/s00382-011-1259-y.

Wang JW, Wang K, Pielke RA, Lin JC, Matsui T (2008) Towards a robust test on North America warming trend and precipitable water content increase. *Geophysical Research Letters **35***: L18804, doi:10.1029/2008GL034564

Watanabe S, Hajima T, Sudo K, Nagashima T, Takemura T, Okajima H, Nozawa T, Kawase H, Abe M, Yokohata T, Ise T, Sato H, Kato E, Takata K, Emori S, and Kawamiya M. 2011: MIROC-ESM 2010: model description and basic results of CMIP5-20c3m experiments. *Geoscientific Model Development* **4**, 845-872. doi:10.5194/gmd-4-845-2011.

Xiao-Ge X, Tong-Wen W, Jie Z. 2013. Introduction of CMIP5 Experiments Carried out with the Climate System Models of Beijing Climate Center. *Advances in Climate Change Research* **4**: 41-49. doi: 10.3724/SP.J.1248.2013.041.

Ye H, Fetzer EJ, Wong S, Behrangi A, Olsen ET, Cohen J, Lambrigtsen BJ, Chen L (2014). Impact of increased water vapor on precipitation efficiency over northern Eurasia. *Geophysical Research Letters* **41**: 2941–2947. DOI: 10.1002/2014GL059830.

Yukimoto S, Yoshimura H, Hosaka M, Sakami T, Tsujino H, Hirabara M, Tanaka TY, Deushi M, Obata A, Nakano H, Adachi Y, Shindo E, Yabu S, Ose T and Kitoh A 2011 Meteorological Research Institute-Earth System Model v1 (MRI-ESM1) - Model Description. Technical Report of MRI, No. 64, 83 pp.

Zorita E, Von Storch H. 1999. The Analog Method as a Simple Statistical Downscaling Technique: Comparison with More Complicated Methods. *Journal of Climate* **12**: 2474–2489.

FIGURE CAPTIONS

Figure 1. (Left) Location of the available rain gauges and its historical maximum daily precipitation. (Right) The 144 rain gauges selected for this study: for a return period of 100 years, the ones with an expected daily precipitation over 250 mm.

Figure 2. Boxplot for every rain gauge of the Mean Normalised Absolute Error (MNAE) between the fitted CDF and the original ECDF of the observed (left) and simulated by downscaling (right) series, for the five used theoretical distributions and for the best one in each case.

Figure 3. (Left) Expected maximum precipitation in a day for several return periods (10, 20, 50 and 100 years) according to the observations and simulations of downscaled ERA40, both uncorrected and corrected. (Right) Bias of the uncorrected and corrected simulations respect to observed time-series.

Figure 4. Validation of the studied climate models: (Left) Extreme precipitation for several return periods. (Right) Bias of the same extreme precipitation, when compared with the extended observations (white colour).

Figure 5. Expected change of extreme precipitation associated with a return period of 10 years, and the statistical significance of this change (p-values according to KS test), for two emission scenarios: (Left) RCP4.5 (Right) RCP8.5. In the lower panels, detail of the densest area (Valencia). Black circles show the places with significant change (p-value > 0.95) according to KS test, while green circles uses ST test.

Figure 6. The same as Fig. 5 but for the return period of 100 years.

FIGURES

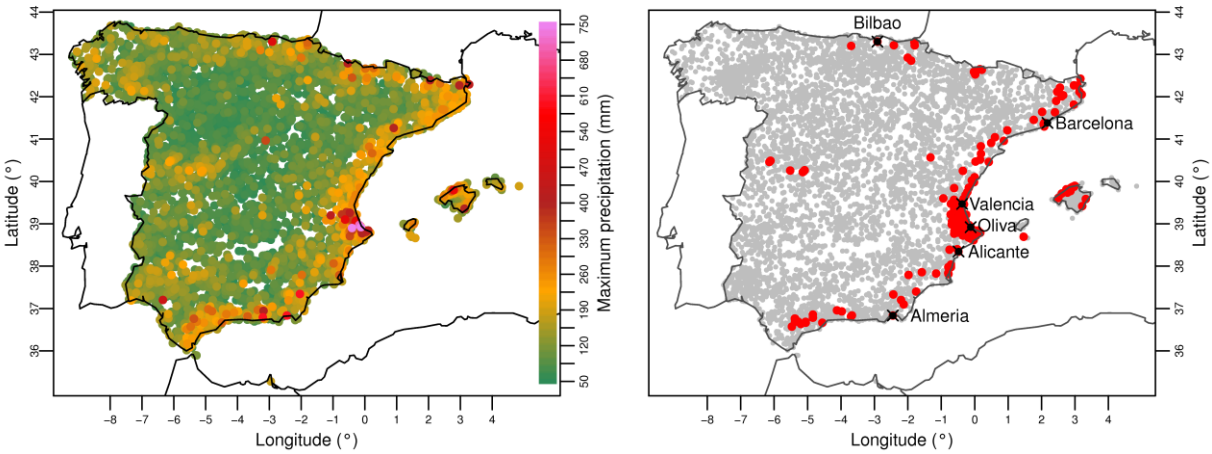

Figure 1. (Left) Location of the available rain gauges and its historical maximum daily precipitation. (Right) The 144 rain gauges selected for this study: for a return period of 100 years, the ones with an expected daily precipitation over 250 mm.

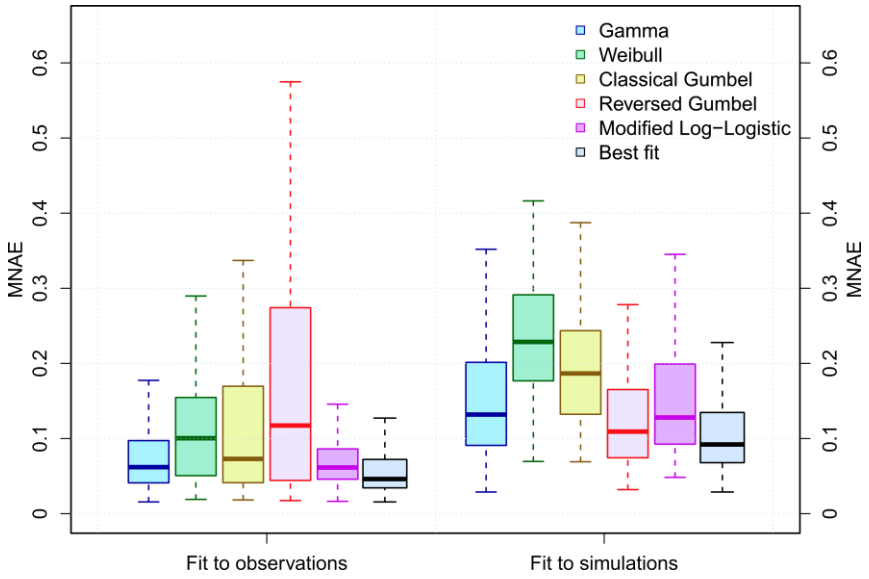

Figure 2. Boxplot for every rain gauge of the Mean Normalised Absolute Error (MNAE) between the fitted CDF and the original ECDF of the observed (left) and simulated by downscaling (right) series, for the five used theoretical distributions and for the best one in each case.

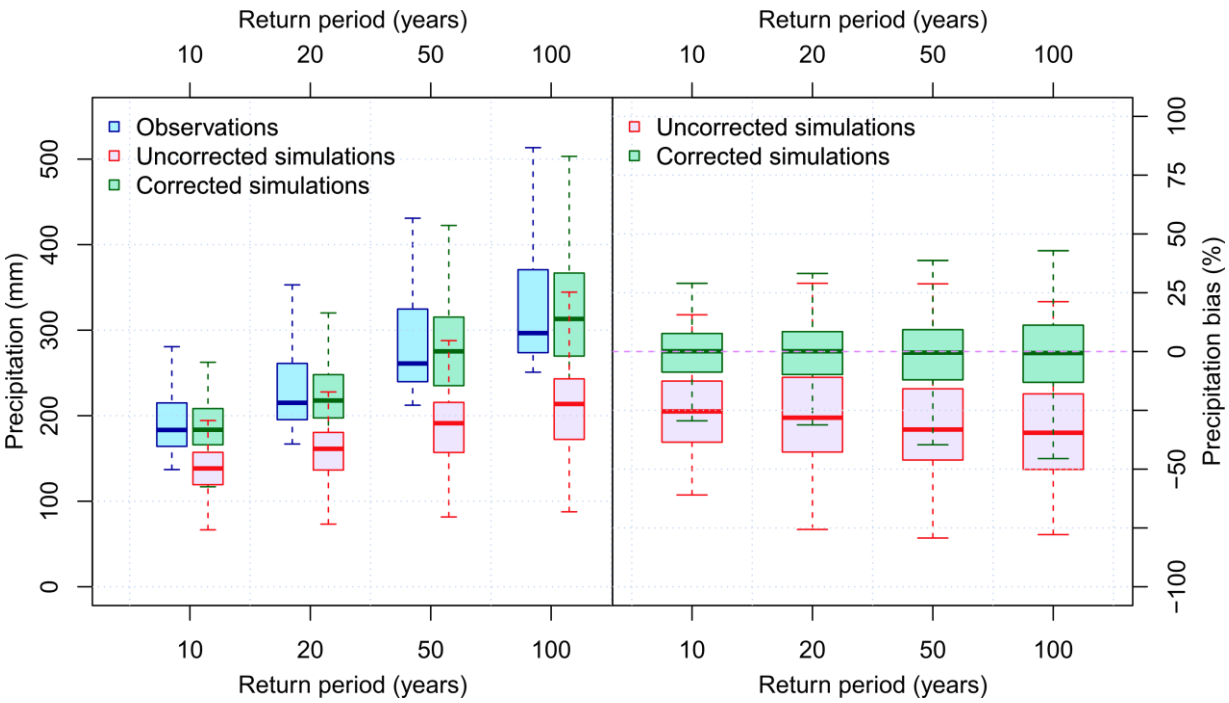

Figure 3. (Left) Expected maximum precipitation in a day for several return periods (10, 20, 50 and 100 years) according to the observations and simulations of downscaled ERA40, both uncorrected and corrected. (Right) Bias of the uncorrected and corrected simulations respect to observed time-series.

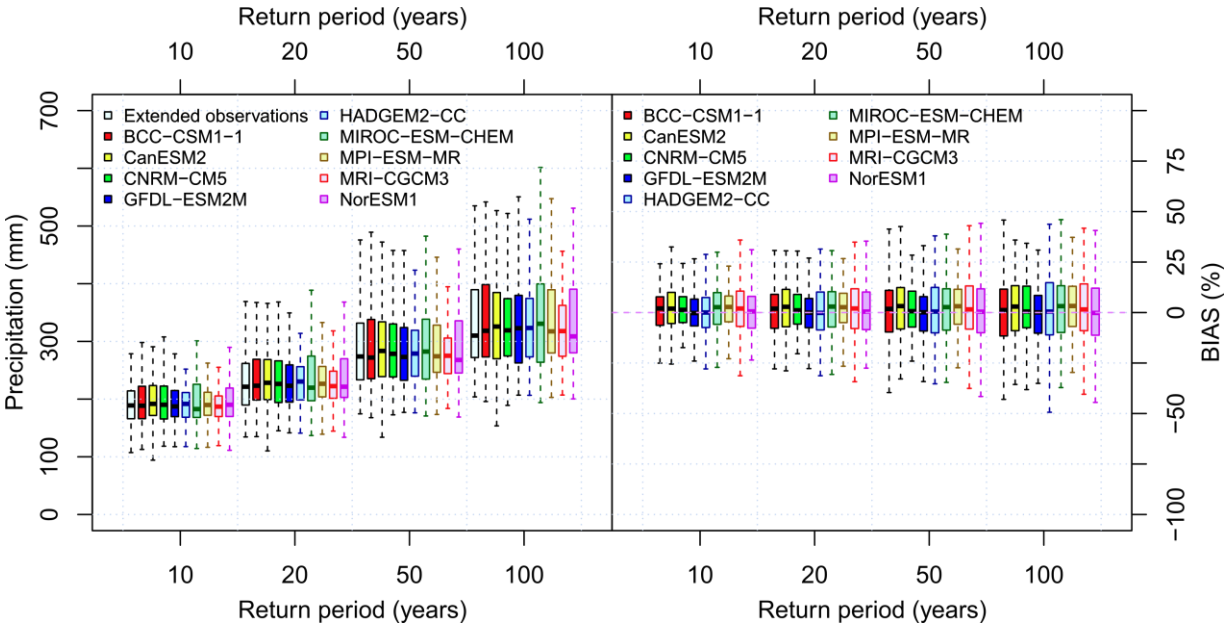

Figure 4. Validation of the studied climate models: (Left) Extreme precipitation for several return periods. (Right) Bias of the same extreme precipitation, when compared with the extended observations (white colour).

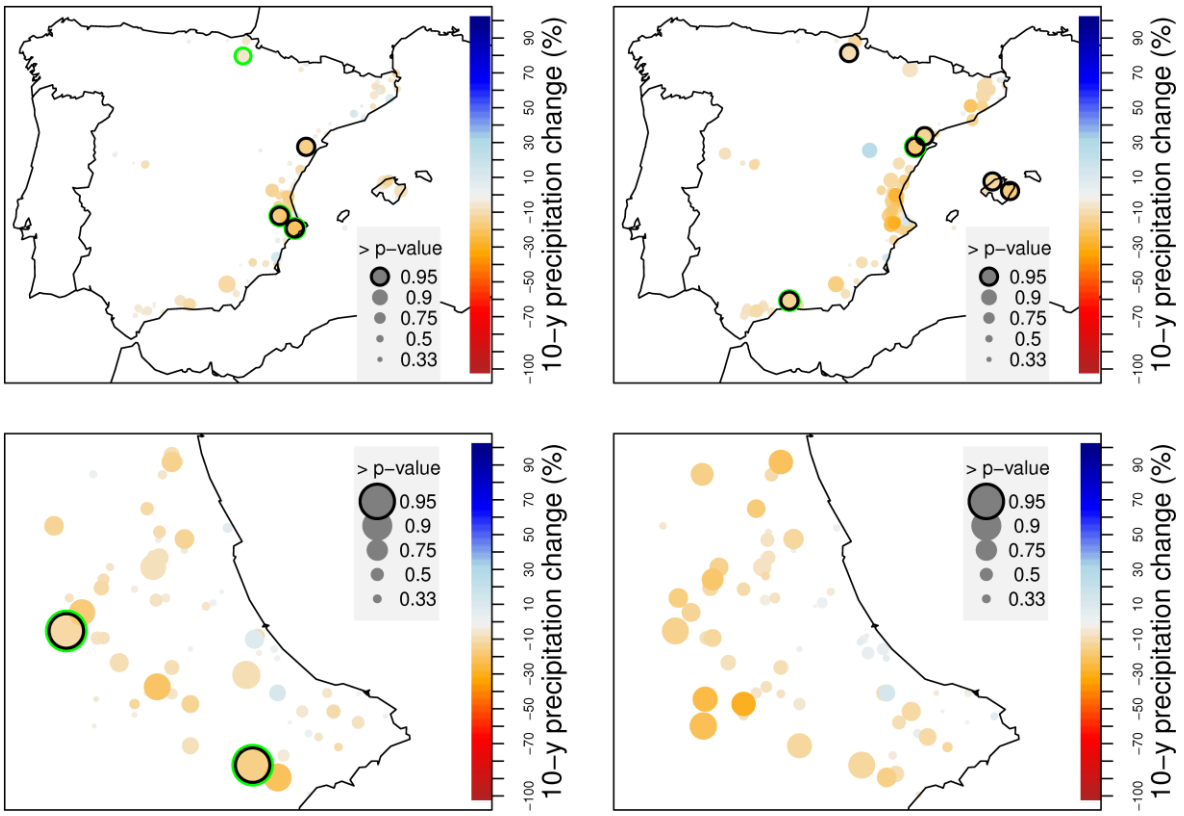

Figure 5. Expected change of extreme precipitation associated with a return period of 10 years, and the statistical significance of this change (p-values according to KS test), for two emission scenarios: (Left) RCP4.5 (Right) RCP8.5. In the lower panels, detail of the densest area (Valencia). Black circles show the places with significant change (p-value > 0.95) according to KS test, while green circles uses ST test.

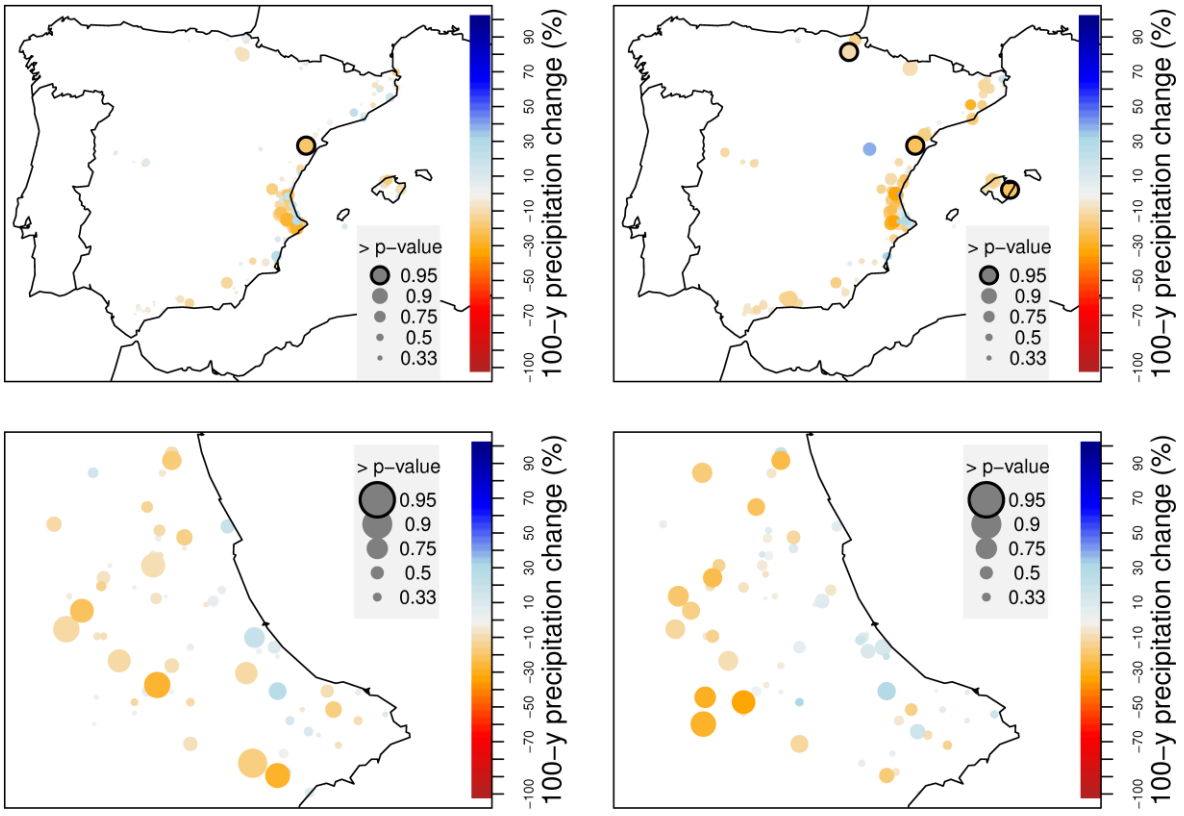

Figure 6. The same as Fig. 5 but for the return period of 100 years.